Theoretical study of the magnetic properties of BaNiF4

Julien Lévêque, Elisa Rebolini, Andrés Saúl, Marie-Bernadette Lepetit

Eur. Phys. J. B manuscript No.
(will be inserted by the editor)

Theoretical study of the magnetic properties of $BaNiF_4$

Julien Lévêque [a,1,2], **Elisa Rebolini** [b,3], **Andrés Saúl** [c,1], **Marie-Bernadette Lepetit** [d,2,3]

[1] Aix-Marseille University, Centre Interdisciplinaire de Nanoscience de Marseille-CNRS (UMR 7325), Marseille, France
[2] Institut Néel, CNRS-UPR 2940, 25 av. des Martyrs, BP 166, 38042 Grenoble Cedex 9, France
[3] Institut Laue Langevin, 71 av. des Martyrs, CS 20156, 38042 Grenoble Cedex 9, France

October 26, 2021

Abstract In this article we study the magnetic properties of the $BaNiF_4$ compound using *ab-initio* calculations and classical Monte-Carlo methods. We discuss the physical origin of the long range magnetic order. We show that the leading exchange interactions are those of a non-frustrated anisotropic two-dimensional Heisenberg system and that long range order and the experimentally observed preferential orientation of the magnetic moments along the **b** axis appear when local single-ion anisotropy contributions are added at first order. We also show that a canting of the magnetic moments appears at second order and can be written as an effective Dzyaloshinskii-Moriya interaction.

1 Introduction

Multiferroics materials were first defined as systems in which at least two ferroic orders — among ferroelectricity, ferromagnetism and ferroelasticity — are coupled [1]. Recently, the concept was extended to compounds in which any magnetic order is coupled to ferroelastic or ferroelectric properties, or even sometimes to the dielectric constant. At first the magnetoelectric multiferroics, that present simultaneously an electric polarization and a magnetic order, received little attention despite two independent predictions of their existence by W. C. Röntgen [2] and P. Curie [3]. In the last decades however magnetoelectrics have become a highly-studied topic [4]. This success is due to the wide range of possible applications [5–8] using the modification of a magnetic order by the application of a simple voltage, or reversely the modification of the polarization or the dielectric constant by the application of a magnetic field.

Despite its discovery in 1968 by M. Eibschtitz *et al.* [9] and the identification of a linear magneto-electric effect a few years latter [10, 11], the $BaMF_4$ family (M being a transition metal) received little interest until recently with the revival in the study of multiferroics materials.

All the members of the family (Mg, Mn, Fe, Co, Ni, Cu, Zn) crystallize in a non centro-symmetric orthorhombic structure, space group $Cmc2_1$ (# 36) (see Fig. 1(a) and (b)). They are all polar (as can be seen from their crystallographic symmetry) with a spontaneous and quite large polarization at room temperature measured using a pulse-field technique, ranging between 7 and 10 $\mu C/cm^2$ depending on the transition metal [12]. All the compounds remain polar up to the melting temperature, the polarization being, in all cases, along the **c** axis. Some members of the family (Mg, Co, Ni, Cu, Zn) are ferroelectric, i.e., the polarization can be reversed with an electric field while in others (Mn and Fe) it cannot be switched [12]. The crystalline structure can be seen as the distortion of a parent centro-symmetric *Cmcm* (# 63) structure, where the MF_6 octahedra (see Fig. 1(a)) appear unrotated, and the Ba atoms occupy the non-polar positions : $z = 0$ and 0.5. As there are two possible ways to rotate the octahedra along the **a** axis [13, 14], the switching of the dipolar moment is associated to these two energetically equivalent possibilities. The impossibility to reverse the polarization in the Mn and Fe compounds was ascribed, by E. T. Keve et al [13, 14], to steric arguments.

The leading magnetic interactions in the magnetic members of the family (Mn, Fe, Co, Ni, Cu) are antiferromagnetic (AFM). Long range AFM order appears below 26.4 K for the $BaMnF_4$ compound [15], 54.2 K for $BaFeF_4$ [16], 69.6 K for $BaCoF_4$ [17], and 68.4 K for $BaNiF_4$ [18] while $BaCuF_4$ shows one-dimensional AFM behavior with no ex-

[a] e-mail: julien.leveque@neel.cnrs.fr
[b] e-mail: rebolini@ill.fr
[c] e-mail: saul@cinam.univ-mrs.fr
[d] e-mail: Marie-Bernadette.Lepetit@neel.cnrs.fr

perimental evidence of long-range ordering [19] despite some authors claiming a Néel temperature of 275 K [20].

In this work we are interested in the magnetic properties of $BaNiF_4$. In this system susceptibility measurements showed that the spin direction lies along the **b** axis [21]. Neutron scattering experiments, performed at 4.2 and 77 K, showed that the AFM magnetic order has a propagation vector $q_M = (\frac{1}{2}, \frac{1}{2}, 0)$ at low temperature [21]. At higher temperatures a broad maximum is observed in the magnetic susceptibility that is sometimes attributed to a two-dimensional ordering [22]. C. Ederer *et al.* [23] predicted the existence of a small canting of the magnetic moments in $BaNiF_4$ which has its origin in the polar distortion, through a proposed Dzyaloshinskii-Moriya (DM) interaction. This canting produces an additional weak antiferromagnetism in the (**a**, **c**) plane. More recently, A. C. Garcia-Castro *et al.* [20] showed that the same canting of the magnetic moments, due to an effective DM interaction coupled to the polar character of the system, also takes place in the $BaCuF_4$ compound. It results in the possibility to reverse, in both systems, this canting order parameter using an electric field [24].

In this article we will study the magnetic properties of the $BaNiF_4$ compound using *ab-initio* calculations and classical Monte-Carlo methods. We will discuss the physical origin of the long-range magnetic order, the preferential orientation of the spins along the **b** direction, and the physical origin of the small canting. We will show that, the preferential orientation of the magnetic moments along the **b** axis appears as a first-order cooperative compromise between the local single-ion anisotropy contributions and the AFM Heisenberg interactions. We will also show that the canting of the magnetic moments appears at second order, and can be written as an effective Dzyaloshinskii-Moriya interaction.

In Section 2 we present the details of the computational methods used in this work. Section 3 will be devoted to the results and discussion. More precisely, in Section 3.1 we present results of the calculations of the effective exchange interactions, in Section 3.2 the single-ion anisotropy, and in Section 3.3 the magnetic order at zero and finite temperature.

2 Computational details

2.1 Crystal structure

At room temperature, $BaNiF_4$ has an orthorhombic structure, space group $Cmc2_1$ (# 36) with lattice parameters a = 4.137 Å, b = 14.431 Å, and c = 5.781 Å [25]. There are four $BaNiF_4$ units in the orthorhombic $Cmc2_1$ unit cell, giving a total of 24 atoms. The C-centering means that the unit cell is not primitive because there are two equivalent crystallographic patterns, one at (0, 0 ,0) and the other at (1/2, 1/2, 0) (see Fig. 1(a) and (b)). The transition metal ions are located in NiF_6 corner-sharing octahedra. These octahedra form puckered layers along the $(\mathbf{a},\mathbf{c})$ directions. The planes are separated along the **b** direction by the Ba atoms and the successive layers are shifted by half a translation vector **a** (see Figure 1(a) and (b)). All the Ni and Ba atoms are equivalent by symmetry, while there are four kinds of F atoms. The primitive cell of the base centered orthorhombic lattice is given by $\mathbf{a}_m = (a,0,0)$, $\mathbf{b}_m = (-a/2,b/2,0)$, $\mathbf{c}_m = (0,0,c)$, and $\gamma = \arccos(-a/\sqrt{a^2+b^2}) = 105.996^\circ$ and contains 12 atoms. It looks like a monoclinic $P2_1$ cell, except that γ is fixed by the orthorhombic space group. The magnetic structure with a propagation vector $(\frac{1}{2}, \frac{1}{2}, 0)$ proposed by Cox *et al.* [21] is shown in Fig. 1(d) in a $2\times2\times1$ supercell (12 Ni atoms in the supercell). It is interesting to note that the same magnetic order can be represented in a $2\times1\times1$ super-cell (4 Ni atoms in the supercell) of the primitive pseudo-monoclinic cell (see Fig. 1(e)).

2.2 *Ab-initio* calculations

The magnetic effective exchange interactions were obtained using multi-reference *ab-initio* calculations of the magnetic spectrum on properly chosen fragments of the crystal. These fragments were embedded in a total ions pseudopotential (TIP) bath [26], that reproduces the exclusion effects of the electronic structure of the two first layers of surrounding atoms, and a renormalized set of charges reproducing the Madelung potential seen by the fragment (see reference [27] for more details). The latter was computed with an error of less than 0.1 meV. The *ab-initio* spectroscopic calculations were performed using the selected active space + single-excitations (SAS+S) method [28] as implemented in the RelaXE code [29]. This method is a multi-reference configuration interaction method (MRCI) that treats exactly the correlation energy within the 3d shell, the ligand to metal charge transfers and screening effects on all configurations so generated. The fragment are chosen to include the magnetic atoms under consideration, their first coordination shell, and any additional bridging ligands. The fragment orbitals were optimized within a complete active space self consistent field (CASSCF) [30] calculation of the 3d electrons, using the MOLCAS package [31]. We used a basis set of $3\zeta+P$ quality, associated to relativistic core pseudopotentials of the Stuttgart group [32] to represent the inner orbitals. The anisotropy calculations were performed using the same method (on a single ion embedded cluster) and the RASSI/ANISO [33] modules of MOLCAS.

The effective exchange interactions were double checked using density functional theory (DFT). A broken-symmetry formalism [34–40] has been used to map total energies corresponding to various collinear spin arrangements within a supercell, onto a Heisenberg Hamiltonian. The calculations

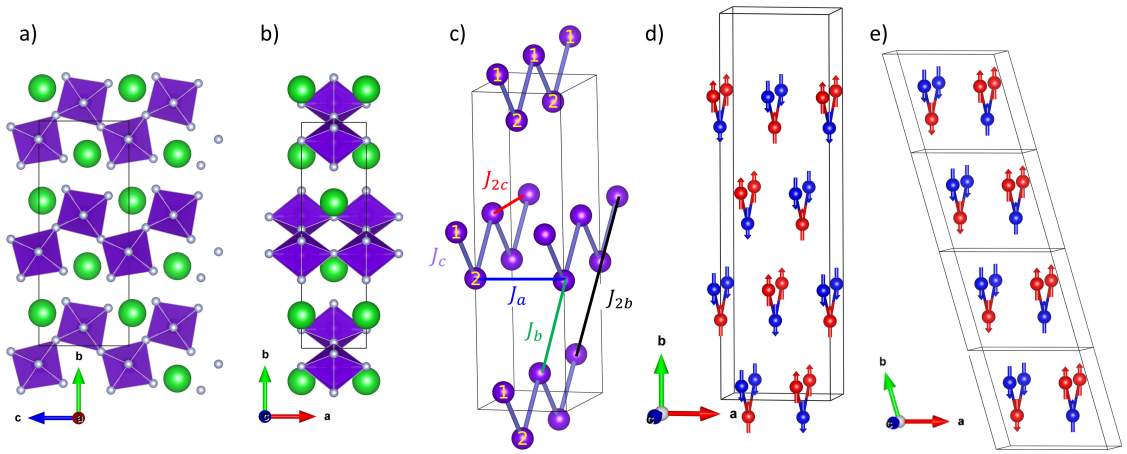

Fig. 1 Schematic representation of the crystal structure of $BaNiF_4$ a) along the **a** and b) **c** axes. The Ba atoms are in green, the Ni in violet and the F in light gray. c) Naming of the magnetic interactions. For the sake of clarity, only the Ni atoms are shown. The first and third neighbors interactions J_c and J_{2c} form a $J_1 - J_2$ one-dimensional system along the **c** axis. The second neighbors interaction J_a connects the chains along the **a** axis and the two effective exchange interactions J_b and J_{2b} connect the adjacent planes along the **b** axis. The numbers 1 and 2 label atoms which are symmetry related by the glide 2_1 rotation along the **c** axis (seet text). Experimental magnetic structure proposed by Cox el al [21] represented d) as a $2\times2\times1$ orthorhombic super-cell and e) as a $2\times1\times1$ monoclinic cell.

were done with the `wien2k` code [41] and a PBE0 functional [42] on a $2\times1\times2$ supercell (containing 96 atoms).

The crystal structure used in all calculations was obtained from the room temperature X-Ray refinement data of reference [25].

2.3 Monte Carlo calculations

Monte Carlo simulations were performed to calculate order parameters and critical temperatures from a model magnetic Hamiltonian derived from the computed *ab-initio* parameters (effective exchange interactions and single ion anisotropies) and dipolar interactions. For this purpose we used the standard Metropolis algorithm [43] on a classical approximation of the spin Hamiltonian. The calculations were performed using up to $200\times1\times100$ orthorhombic supercells, containing 80000 Ni atoms, and $20\times10\times10$ supercells containing 8000 atoms when the dipolar contribution was included in the total energy. Thermodynamical averages have been performed with 1250 Monte Carlo steps per atom.

3 Results and discussion

3.1 Magnetic interactions

The magnetic exchange interactions were obtained from the *ab-initio* calculations by mapping the computed magnetic spectra onto the energy spectra of an Heisenberg Hamiltonian on the same fragments :

$$\hat{H} = -\sum_{i>j} J_{ij}\, \hat{\mathbf{S}}_i \cdot \hat{\mathbf{S}}_j, \qquad (1)$$

where the effective exchange interactions J_{ij} are the two intra-chain interactions, J_c and J_{2c}, the inter-chain interaction, J_a, and two interactions J_b and J_{2b} connecting the adjacent planes along the **b** axis (see Fig. 1(c)). A positive (negative) value corresponds to a ferromagnetic (antiferromagnetic) interaction.

The Ni ion has a +2 formal charge, corresponding to a $3d^8$ electronic configuration, with two magnetically active orbitals and a $S = 1$ spin . The two magnetic orbitals are the e_g orbitals of the distorted octahedral environment. The first orbital, shown in Fig. 2(a), is the $d_{x^2-y^2}$ orbital (in the $(\mathbf{b},\mathbf{c})$ plane). It is expected to be responsible for the intra-chain interactions J_c and J_{2c} (see Fig. 1(c)). The second orbital, shown in Fig. 2(b), is the $d_{3z^2-r^2}$ orbital oriented along the **a** axis. It is expected to be responsible for the inter-chain interaction J_a.

The corresponding Ni-Ni distances associated to the effective interactions are shown in Table 1 along with the magnetic integrals obtained from our *ab-initio* calculations. The leading interactions J_c and J_a are both antiferromagnetic and they do not lead to frustration. The effective magnetic exchanges between the planes, J_b and J_{2b}, are negligible. Similarly the magnetic frustration associated with the second neighbors interaction within the chains running along the **c** direction, J_{2c}, is negligible. Its value is within the estimated error bar of our method.

The two leading AF interactions are consistent with the experimental magnetic order shown in Fig. 1. As they form a 2-dimensional pattern, alone they cannot give rise to a long-range order [44]. Other interactions must be included in our model Hamiltonian to explain a possible two-dimensional long-range magnetic order [45] and even more to account for

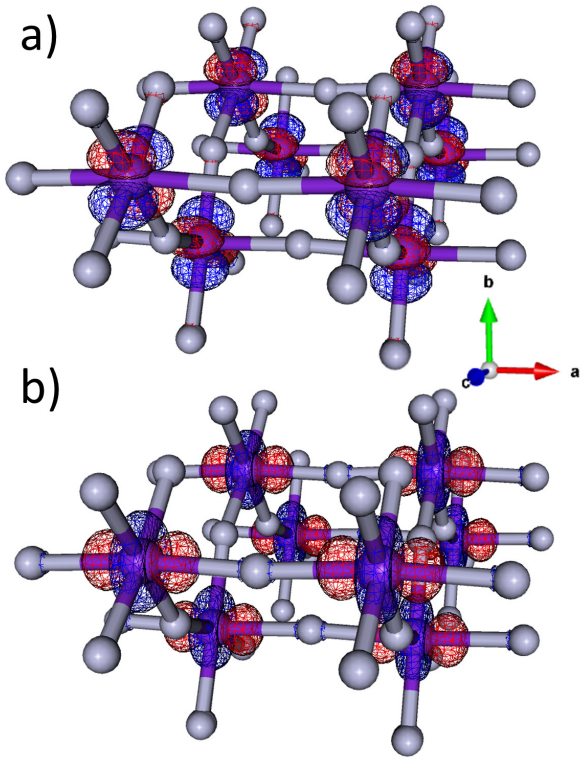

Fig. 2 Magnetic orbitals obtained from the CASSCF calculation. a) $d_{x^2-y^2}$ orbital responsible for the magnetic couplings along the chains running on the **c** direction (view in the (**b**, **c**) plane). b) $d_{3z^2-r^2}$ orbital responsible for the magnetic couplings along the **a** direction (view in the (**b**, **a**) plane).

J	d [Å]	J [meV] SAS+S	J [K] SAS+S	J[K] PBE0	J [K] [23] LSDA+U
J_c	3.840	-3.855	-44.72	-52	-77
J_a	4.137	-6.373	-73.93	-102	-102
J_{2c}	5.781	-0.016	-0.19	-2	
J_b	5.882	0.001	0.01	0	
J_{2b}	7.506	0.001	0.01	0	

Table 1 Effective exchange interactions. The five interactions calculated in this work between the Ni atoms obtained using the *ab-initio* and density functional theory methods are listed in the first column. The label of the different J values can be found in Fig. 1(c). The Ni-Ni distances appear in the second column. The third and fourth columns give the interactions calculated with the SAS+S method in [meV] and [K], the fifth and sixth the ones calculated with DFT based methods in this work and by Ederer et al [23]. A negative value is associated with an antiferromagnetic interaction (see text and Eq. (1)).

the three-dimensional one proposed by some authors [21] for the transition at 68.4 K.

3.2 On-site anisotropy

As mentioned above, neutron scattering experiments [21] show a preferential orientation of the spins along the **b** direction. To understand the origin of this preference, we computed the site easy axes and the zeroth-field splitting tensor on embedded NiF_6 clusters.

The zeroth-field splitting tensor can be derived from the eigenstates and energies of the many-body, *ab-initio*, electronic plus spin-orbit Hamiltonian on the NiF_6 embedded fragment, using the pseudo-spin method of L. Ungur and L. F. Chiboratu [33]. The result can be written as :

$$\hat{H}_{\rm ZFS} = \mathscr{D}\left[(\hat{\mathbf{S}}\cdot\mathbf{Z})^2 - \frac{S(S+1)}{3}\right] + \mathscr{E}\left[(\hat{\mathbf{S}}\cdot\mathbf{X})^2 - (\hat{\mathbf{S}}\cdot\mathbf{Y})^2\right] \quad (2)$$

where **X**, **Y**, and **Z** are the main anisotropy directions. As in our case, $\mathscr{D}$ = 0.8430 meV = 9.782 K and $\mathscr{E}$ = -0.0936 meV = -1.086 K, **X** and **Z** are the easy and hard directions respectively. Due to the glide 2_1 axis around **c**, the zig-zag chains along the **c** axis are formed by two sets of atoms, labeled 1 and 2 on Figures 1(c) and 3. The local directions of the main anisotropy axes for the two Ni atoms transform into each other by the same symmetry operation. The expansion of the main anisotropy axes onto the crystallographic ones is provided in Table 2.

Site	Anisotropy axes	**a**	**b**	**c**
1	**X**	0.000	-0.746	0.666
	Y	0.000	0.666	0.746
	Z	1.000	0.000	0.000
2	**X**	0.000	0.746	0.666
	Y	0.000	0.666	-0.746
	Z	1.000	0.000	0.000

Table 2 Coordinates of the main anisotropy axes in the crystallographic basis for the two Ni atoms related by the 2_1 symmetry (see Fig 3).

The hard axis **Z** is along the **a** direction for the two atoms. The other main anisotropy axes for the two Ni atoms, **X** and **Y**, are nearly orthogonal and lay in the (**b**, **c**) plane. It is interesting to note that the easy axes **X** (in red on Fig 3) are nearly parallel to the shortest Ni-F bonds (in black on Fig 3). Figure 4(a) shows the anisotropy contributions of the two Ni atoms for different orientations. **a** is clearly the hard direction for both atoms and different contributions appear when rotating the spins from **b** to **c** with a local maximum for Ni_1 and a local minimum for Ni_2 (blue and red curves respectively in Fig. 4(a)). Similar but inverted curves (minimum for Ni_1 and maximum for Ni_2) would appear if we rotate the spins from **c** to $-$**b** (not shown in Fig. 4(a)).

For the two Ni atoms forming the chain, the easy axes (corresponding to the local minima mentioned before) are rotated clockwise and anti-clockwise by an angle $\alpha = 41.75°$ with respect to the **b** axis. In this way we can write :

$$\mathbf{X}_1 = \cos\alpha\,\mathbf{b} - \sin\alpha\,\mathbf{c}, \qquad \mathbf{Y}_1 = \sin\alpha\,\mathbf{b} + \cos\alpha\,\mathbf{c}, \quad (3)$$

$$\mathbf{X}_2 = \cos\alpha\,\mathbf{b} + \sin\alpha\,\mathbf{c}, \qquad \mathbf{Y}_2 = \sin\alpha\,\mathbf{b} - \cos\alpha\,\mathbf{c}. \quad (4)$$

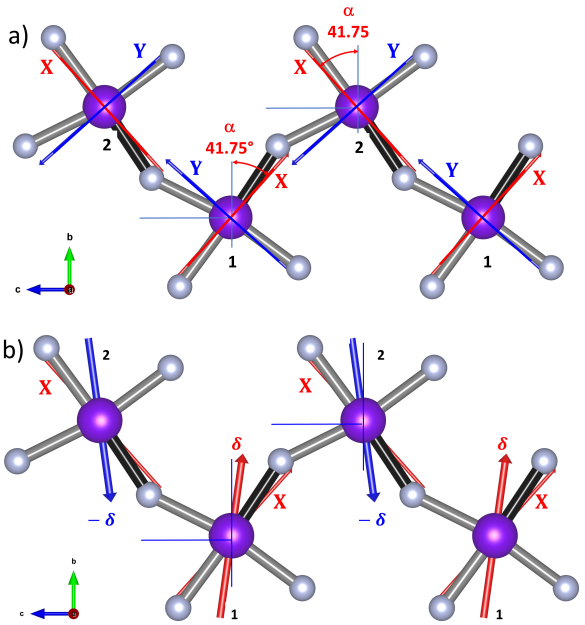

Fig. 3 (color online) Chains along the **c** axis. Ni atoms are shown in violet and the F atoms in light gray. The shortest Ni-F bond (1.95 Å) is colored in black. Atoms labeled 1 and 2 are symmetry related by the glide 2_1 rotation along the **c** axis. a) The Ni easy axes **X** are represented with red lines, and the other main anisotropy direction in the (**b**, **c**) plane **Y** in blue. The hard axes **Z** are perpendicular to the figure. α is the angle between the local easy axes **X** and the **b** direction. b) Spins orientation corresponding to the minimum energy solution of the two-dimensional classical Heisenberg plus zeroth-field splitting Hamiltonian (Eq. (7)). The preferred orientation is along the **b** direction with a small tilt δ (see text).

The sum of the two contributions, which corresponds to a collinear rotation of the two spins, is shown in black in Fig. 4(a), it gives a local minimum along the **b** direction (see below).

3.3 Magnetic order

We will first discuss the magnetic order at zero temperature considering a classical Heisenberg plus zeroth-field splitting model with a unit cell formed by the two symmetry related Ni spins. As any projection of the spins along the **a** direction increases the anisotropy contribution (Fig. 4(a) and Eq. (2)), we will search the solutions of a two-dimensional model with the spins in the (**b**, **c**) plane :

$$\mathbf{S}_1 = \sin\theta_1\ \mathbf{b} + \cos\theta_1\ \mathbf{c}, \tag{5}$$

$$\mathbf{S}_2 = \sin\theta_2\ \mathbf{b} + \cos\theta_2\ \mathbf{c} \tag{6}$$

here θ_i are the angles formed with respect to the **c** axis. The Heisenberg and single ion anisotropy contributions to the total energy per unit cell can be written as :

$$E(\theta_1,\theta_2) = 2\,J_a\,S^2 - 2\,J_c\,S^2\cos(\theta_2-\theta_1) - \mathscr{D}\frac{2\,S\,(S+1)}{3} - \mathscr{E}\,S^2\left[\cos 2(\theta_1-\alpha)+\cos 2(\theta_2+\alpha)\right], \tag{7}$$

where we assume an AFM order between the chains along the **a** axis independently of the angles θ_i, as the exchange interaction J_a is larger than the on site anisotropy $\mathscr{E}$.

In the limit of $\mathscr{E}=0$, the minimum energy

$$E_{\rm AFM} = 2\,J_a\,S^2 + 2\,J_c\,S^2 - 2\,\mathscr{D}\frac{S\,(S+1)}{3} \tag{8}$$

is obtained for the in-plane, rotation-invariant, AFM collinear solution along the chains ($\theta_2-\theta_1=\pi$).

A finite $\mathscr{E} << J_c$ breaks the in plane rotation symmetry. At first order in $\mathscr{E}$, a collinear AFM minimum is obtained with the spins oriented along the **b** direction: $\theta_1 = -\theta_2 = \pi/2$ (see black curve in Fig. 4(a)), in good agreement with the experimental observation. The first order energy is :

$$E^1_{\rm AFM} = E_{\rm AFM} + 2\,\mathscr{E}\,S^2\,\cos 2\alpha \tag{9}$$

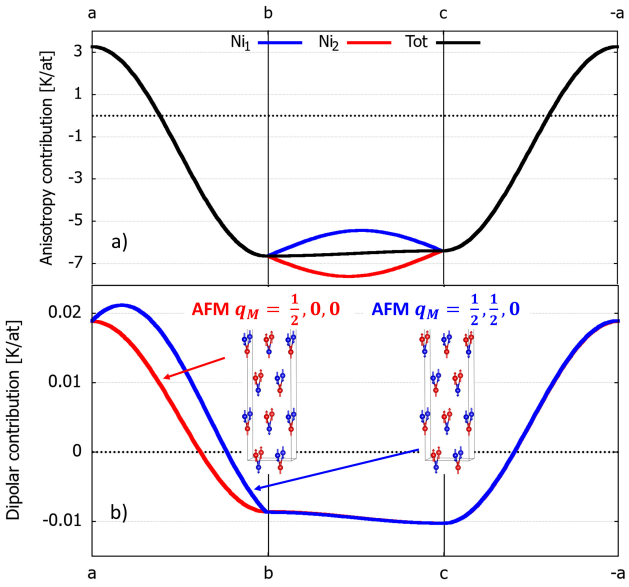

Fig. 4 (color online) Energy contribution due to (a) the single ion anisotropy and (b) the dipolar interactions for collinear magnetic arrangements. The single ion anisotropy contribution is shown for the two symmetry related Ni atoms separately (Ni_1 (blue) and Ni_2 (red)) and its sum (black). The dipolar contribution is shown for the two AFM arrangements that minimize the Heisenberg exchange interactions. They correspond to $(\frac{1}{2},0,0)$ (red) and $(\frac{1}{2},\frac{1}{2},0)$ (blue) propagation vectors. The spins orientation are within the $(\mathbf{a},\mathbf{b})$ plane in the left part, within the $(\mathbf{b},\mathbf{c})$ plane in the middle part and within the $(\mathbf{a},\mathbf{c})$ plane in the right part.

At second order in $\mathscr{E}$, an additional energy gain can be obtained with a small non-collinear tilt of the spins: $\theta_1 = \pi/2+\delta$ and $\theta_2 = -\pi/2-\delta$, where

$$\tan 2\delta = \frac{\mathscr{E}\sin 2\alpha}{\mathscr{E}\cos 2\alpha + J_c} \tag{10}$$

and

$$\delta \simeq \frac{\mathscr{E}}{2J_c}\sin 2\alpha \simeq 0.7^\circ \tag{11}$$

The second order energy becomes :

$$E^2_{\rm AFM} \simeq E_{\rm AFM} + 2\,J_c\,S^2\,(\cos 2\delta - 1) + 2\,\mathscr{E}\,S^2\,\cos(2\alpha - 2\delta)$$
$$\simeq E_{\rm AFM} + 2\,\mathscr{E}\,S^2\,\cos 2\alpha + \frac{\mathscr{E}^2\,S^2\,\sin^2 2\alpha}{J_c} \qquad (12)$$

As we showed in Fig. 5, this solution corresponds to an AFM order, with the spins oriented very close to the **b** direction. The small tilt represents a tiny canting as shown schematically (not in scale) in Figures 3(b) and 5(b). The time inverted configuration, $\theta_1 = 3\pi/2 + \delta$ and $\theta_2 = \pi/2 - \delta$, is also an energy minimum with the same energy. These two solutions appear alternatively in parallel chains along **a**, as expected for a $(\frac{1}{2},\frac{1}{2},0)$ propagation vector (see Fig. 5). The tilt thus generates weak ferromagnetism along the chains

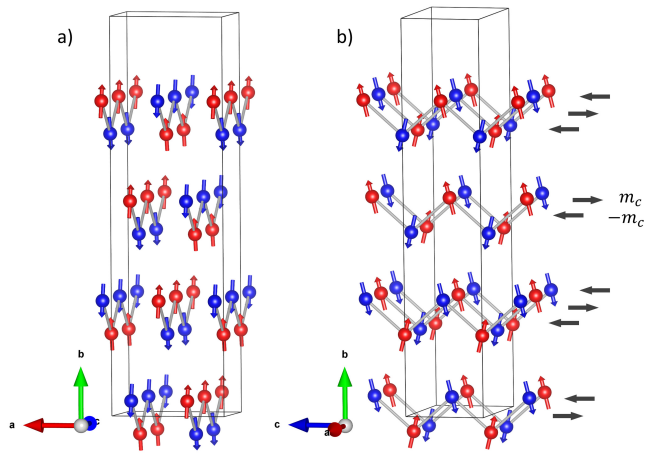

Fig. 5 Magnetic order with tilt. View along the a) **c** and along the b) **a** axes. There is a weak ferromagnetic order along the chains that generates a small magnetic moment along the **c** axis (see text). The magnetic moment for each chain in panel b) is represented by a small black arrow in the right part of the figure. The crystal symmetry precludes the existence of a net measurable macroscopic magnetization.

(see Fig. 5(b)), with a net magnetic moment per unit cell (two Ni atoms) :

$$\mathbf{m} = -2\,S\,\sin\delta\,\mathbf{c} \simeq -S\,\sin 2\alpha\,\frac{\mathscr{E}}{J_c}\mathbf{c} \qquad (13)$$

It is interesting to remark that these results were obtained considering Heisenberg interactions and single-ion anisotropy terms only while similar results were obtained by Ederer et al [23] for the $BaNiF_4$ compound and A. C. Garcia-Castro *et al.* [20] for the $BaCuF_4$ system using an alternative description with effective single ion anisotropy contributions and a Dzyaloshinskii-Moriya interaction.

It can be shown that these two descriptions, close to the first-order local minimum of energy $E^1_{\rm AFM}$, are perfectly equivalent. In the alternative description, the Hamiltonian would be written as follows :

$$\hat{\tilde{H}} = 2\,J_a\,S^2 - 2\,J_c\,\hat{\mathbf{S}}_1\cdot\hat{\mathbf{S}}_2 - f\,(\mathbf{b}\cdot\hat{\mathbf{S}}_1)^2 - f\,(\mathbf{b}\cdot\hat{\mathbf{S}}_2)^2$$
$$+\,g\,\mathbf{a}\cdot(\hat{\mathbf{S}}_1\times\hat{\mathbf{S}}_2). \qquad (14)$$

where $f, g > 0$. Assuming, once again, that the spins lay in the (**b**, **c**) plane, the energy for the two Ni atoms unit cell can be written as :

$$\tilde{E}(\theta_1,\theta_2) = 2\,J_a\,S^2 - 2\,J_c\,S^2\cos(\theta_2-\theta_1) \qquad (15)$$
$$-\,f\,S^2\,(\sin^2\theta_1 + \sin^2\theta_2) + g\,S^2\,\sin(\theta_1-\theta_2)$$

in this case, the collinear AFM solution with the spins oriented along the **b** direction $\theta_1 = -\theta_2 = \pi/2$ is obtained for $g = 0$, with an energy :

$$\tilde{E}^1_{\rm AFM} = E_2\,J_a\,S^2 + 2\,J_c\,S^2 - 2f\,S^2 \qquad (16)$$

and the non-collinear solution $\theta_1 = -\theta_2 = \pi/2 + \delta$, with :

$$\tan 2\delta = \frac{g}{f - 2J_c} \qquad (17)$$

is obtained at second order in g :

$$\tilde{E}^2_{\rm AFM} \simeq \tilde{E}^1_{\rm AFM} + \frac{S^2\,g^2}{4J_c - 2f} \qquad (18)$$

Finally, comparing the corresponding energies and tilt angles it can be shown that the two models are numerically equivalent if :

$$f \simeq \mathscr{D}\,\frac{S+1}{3\,S} - 2\,\mathscr{E}\,\cos 2\alpha \qquad (19)$$

$$g = \frac{(f - 2\,J_c)\,\mathscr{E}\,\sin 2\alpha}{\mathscr{E}\,\cos 2\alpha + J_c} \simeq -2\,\mathscr{E}\,\sin 2\alpha \qquad (20)$$

where these expressions apply when $|J_c| \gg |\mathscr{E}|, f$. We get $f = 6.64$ K and $g = 2.15$ K. It is interesting to note, that as the effective DM parameter g goes as $\sin 2\alpha$, it is zero, corresponding to a collinear AFM state with no canting, for $\alpha = 0$ (easy axis along **b**) and maximum for $\alpha = \pi/4$.

The single-ion anisotropy breaks the rotation symmetry of the two-dimensional Heisenberg Hamiltonian, and allows the existence of long-range order at low temperatures. Short and long-range order parameters :

$$Sg = \frac{1}{N_{\rm atoms}}\left\| \sum_{\mathscr{P}_{\mathbf{ac}}:\,\text{planes}\,(\mathbf{a},\mathbf{c})}\ \sum_{(i,j)\in\mathscr{P}_{\mathbf{ac}}} (-1)^{i+j}\,\mathbf{S}_{(i,j),\mathscr{P}_{\mathbf{ac}}} \right\|$$

$$LRO_{\mathbf{x}} = \frac{1}{N_{\rm atoms}}\left\| \sum_{\mathscr{C}_{\mathbf{x}}:\,\text{chains along}\,\mathbf{x}}\ \sum_{i\in\mathscr{C}_{\mathbf{x}}} (-1)^{i}\,\mathbf{S}_{i,\mathscr{C}_{\mathbf{x}}} \right\|$$

$$SRO_{\mathbf{x}} = \frac{1}{N_{\rm atoms}}\sum_{\mathscr{C}_{\mathbf{x}}:\,\text{chains along}\,\mathbf{x}}\ \sum_{i\in\mathscr{C}_{\mathbf{x}}} \mathbf{S}_{i,\mathscr{C}_{\mathbf{x}}}\cdot\mathbf{S}_{i+1,\mathscr{C}_{\mathbf{x}}}$$

calculated from the Monte-Carlo simulations, are shown respectively in Figures 6(a), (b), and (c).

As expected the short-range order parameters decrease with temperature. The one along the **c** direction decreases faster that the one along the **a** direction in agreement with the relative strength of the corresponding exchange interactions J_a and J_c (see Fig. 6(c)). The long-range order parameters show a transition temperature near 42 K (see Fig. 6(b)). This transition corresponds to a two-dimensional magnetic order in the (**a**, **c**) plane, with the spins oriented along the

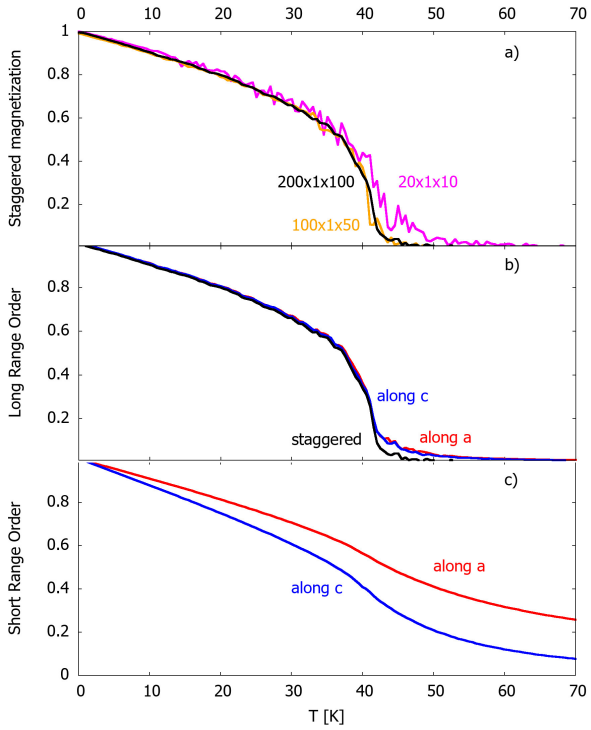

Fig. 6 (color online) Results of Monte-Carlo simulations versus temperature. a) Staggered magnetization for three different orthorhombic supercells $20\times1\times10$ (magenta), $100\times1\times50$ (orange), and $200\times1\times100$ (black) containing respectivelly 800, 20000, and 80000 Ni atoms. b) Staggered magnetization, Sg (black), and long-range order parameters, $LRO_{\mathbf{x}}$, along the **a** (red) and **c** (blue) directions. c) Short-range order parameters, $SRO_{\mathbf{x}}$, along the **a** (red) and **c** (blue) directions. $200\times1\times100$ orthorhombic supercells have been used in b) and c).

b axis. It can be associated to the transition temperature announced in the literature at 68.4 K. The underestimation of the critical temperature can be due to a possible underestimation of the effective exchange interactions but it is more likely due to the classical treatment of the quantum spin S = 1 Hamiltonian which overestimates the entropy contributions to the free energy lowering the critical temperature. Indeed, a calculation with an Ising Hamiltonian and the same exchange interactions results in an underestimation of the entropy contribution and a critical temperature of about 138 K. As the energy difference between collinear and non-collinear configurations is very small (0.026 K/at), the spins can be easily aligned with a small magnetic field, or disoriented at finite temperature. For this reason, no long-range order associated to the tilts was observed in our simulations.

As expected, no order is observed between the planes with a two-dimensional Heisenberg Hamiltonian and a local single ion anisotropy. As in the literature the 68.4 K transition has been associated with a 3D ordering [18, 22], we added dipolar interactions in order to evaluate if some 3D long-range order can be triggered by them. We estimated their energy contribution using the Hamiltonian :

$$\hat{H}_{\text{dip}} = -\frac{\mu_0}{4\pi}\sum_{i>j}\frac{1}{r_{ij}^3}[3\,(\hat{\mathbf{m}}_\mathbf{i}\cdot\mathbf{r}_{ij})\,(\hat{\mathbf{m}}_\mathbf{j}\cdot\mathbf{r}_{ij}) \;-\; \hat{\mathbf{m}}_\mathbf{i}\cdot\hat{\mathbf{m}}_\mathbf{j}] \qquad (21)$$

where μ_0 is the vacuum permeability, $\hat{\mathbf{m}}_\mathbf{i} = g\mu_B\,\hat{\mathbf{S}}_\mathbf{i}$ and $\hat{\mathbf{m}}_\mathbf{j} = g\mu_B\,\hat{\mathbf{S}}_\mathbf{j}$ are the corresponding spin-only magnetic moments, and $\mathbf{r}_{ij}$ the distance vector between them.

There are two AFM magnetic orders compatible with the two leading Heisenberg exchange interactions, J_a and J_c. They respectively correspond to $(\frac{1}{2},0,,0)$ and $(\frac{1}{2},\frac{1}{2},0)$ propagation vectors (see inset in Fig. 4(b)). The dipolar energy contributions to the total energy for these two orders are shown in Fig. 4(b). The dipolar term displays a small preference to align the spins along the **c** axis, but the energy gain is much smaller than the one due to the single-ion anisotropy, that tends to align the spins along the **b** axis (see Fig. 4(a)). Once aligned along the latter, the high level of symmetry in the $Cmc2_1$ space group leaves very small dipolar energy gain (about 0.1 mK/at) to stabilize the $(\frac{1}{2},\frac{1}{2},0)$ magnetic order proposed experimentally. We can hardly argue that this contribution can explain the experimental observation of a three-dimensional order at low temperature. Due to the weakness of the interplane interactions, J_b and J_{2b}, it does not seem more likely that the long-range order could be explained by an order by disorder mechanism [46], due to the spin S = 1 quantum fluctuations. In fact the only possibility seems to be a crystallographic symmetry breaking, removing the $(\mathbf{a}+\mathbf{b})/2$ partial translation relating the two (**a**, **c**) planes in the unit cell. Indeed, this $Cmc2_1$ to $Pmc2_1$ symmetry breaking would allow both magnetic interactions along **b**, exchange and dipolar, to produce a non zero contribution to the total energy allowing the effective interaction between the planes along the **b** axis without modifying their stable two-dimensional AFM order (see Fig 1(d)).

4 Discussion

We showed that the local single-ion anisotropies of the Ni atoms, in conjunction with the AFM Heisenberg interactions, are responsible of the preferred orientation of the spins along the **b** axis, as observed in neutron scattering experiments [21]. A small, non-collinear contribution to the spin order appears as a second order correction of the same Hamiltonian. Due to the odd parity of the arctangent function in Eq. (10) — that can be associated to the broken inversion symmetry along the **c** axis — the sign of the non-collinear tilt is defined by the sign of $\mathscr{E}/J_c$. For every Ni atom, this tilt takes place in order to slightly rotate the spins from the **b** direction toward the local easy axis **X** direction, the latter being very close to the shortest Ni-F bonds as mentioned above. As originally suggested by E. T. Keve et al [13, 14]

and observed by Ederer et al [23] for the $BaNiF_4$ compound and by A. C. Garcia-Castro *et al.* [20] for the $BaCuF_4$ system, the reversal of the electric polarization with an applied electric field will produce an inversion of the rotation of the MF_6 octahedra, thus inverting the sign of the tilt. The weak ferromagnetic magnetic moment along the chains and the overall weak antiferromagnetic order parameter can thus be controlled with an electric field. Indeed, this coupling has been observed by Q. Xu et al [24] for thin film of $BaNiF_4$ deposited on a $Al_2O_3(0001)$ substrate.

5 Acknowledgements

We acknowledge financial support from the ANR HTHPCM. This work was performed using HPC resources from GENCI-IDRIS and CRIANN under project N° 91842 and N° 2007013. AS gratefully acknowledge Gustavo Stolovitzky for fruitful discussions. We acknowledge fruitful discussions with Xavier Rocquefelte, Daniel Braithwaite, and David Vincent.

Author Contribution

JL, MBL, and AS designed the work. ER and MBL developed the ab-initio computational method and codes used to calculate the effective exchange interactions. JL, ER and MBL calculated the effective exchange interactions and single ion anisotropy terms using ab-initio methods. AS calculated the effective exchange interactions using the DFT based methods. JL performed the MC simulations. JL and AS developed the analytical model. JL, MBL, and AS wrote the manuscript. All the authors discussed the results.

References

1. H. Schmid, Multi-ferroic magnetoelectrics, Ferroelectrics **162**(1), 317 (1994)
2. W.C. Röntgen, Ueber die durch Bewegung eines im homogenen electrischen Felde befindlichen Dielectricums hervorgerufene electrodynamische Kraft, Annalen der Physik und Chemie **271**(10), 264 (1888)
3. P. Curie, Sur la symétrie dans les phénomènes physiques, symétrie d'un champ électrique et d'un champ magnétique, Journal de Physique Théorique et Appliquée **3**(1), 393 (1894)
4. M. Fiebig, Revival of the magnetoelectric effect, Journal of Physics D: Applied Physics **38**(8), R123 (2005)
5. Y. Yang, J. Seidel, S.J. Byrnes, P. Shafer, C.H. Yang, M.D. Rossell, P. Yu, Y.H. Chu, J.F. Scott, J.W. Ager, L.W. Martin, R. Ramesh, Above-bandgap voltages from ferroelectric photovoltaic devices, Nat. Nanotechnol. **5**, 143 (2010)
6. J.T. Heron, et al., Deterministic switching of ferromagnetism at room temperature using an electric field, Nature **516**, 370 (2014)
7. N. Ortega, A. Kumar, J.F. Scott, R.S. Katiyar, Multifunctional magnetoelectric materials for device applications, Journal of Physics: Condensed Matter **27**(50), 504002 (2015)
8. N.A. Spaldin, R. Ramesh, Advances in magnetoelectric multiferroics, Nature Materials **18**(3), 203 (2019)
9. M. Eibschtitz, E. Burstein, Antiferromagnetic-piez oelectric crystals: $BaMF_4$ (M = Mn, Fe, Co and Ni), Solid State Communications **6**, 3 (1968)
10. B.I. Al'Shin, D.N. Astrov, A. Tishchenko, S. Petrov, Magnetoelectric effect in $BaCoF_4$, ZhETF Pis. Red. **12**, 206 (1970)
11. B.I. Al'Shin, D.N. Astrov, R.V. Zorin, Low-frequency magnetoelectric resonances in $BaMnF_4$, Zh. Eksp. Teor. Fiz. **63**, 2198 (1972)
12. M. Eibschütz, H. Guggenheim, S. Wemple, I. Camlibel, M. DiDomenico, Ferroelectricity in $BaM^{2+}F_4$, Physics Letters A **29**(7), 409 (1969)
13. E.T. Keve, S.C. Abrahams, J.L. Bernstein, Crystal structure of pyroelectric paramagnetic barium manganese fluoride, $bamnf_4$, The Journal of Chemical Physics **51**(11), 4928 (1969)
14. E.T. Keve, S.C. Abrahams, J.L. Bernstein, Ferroelectric paraelastic paramagnetic barium cobalt fluoride, $BaCoF_4$, crystal structure, J. Chem. Phys. **53**, 3279 (1970)
15. J.F. Scott, Phase transitions in $BaMnF_4$, Reports on Progress in Physics **42**(6), 1055 (1979)
16. M. Eibschütz, L. Holmes, H.J. Guggenheim, D.E. Cox, Magnetic behavior of the two dimensional antiferromagnet $BaFeF_4$, Le Journal de Physique Colloques **32**(C1), C1 (1971)
17. M. Eibschütz, L. Holmes, H.J. Guggenheim, D.E. Cox, Magnetic Structure of the Two-Dimensional Antiferromagnet $BaCoF_4$, Physical Review B **6**(7), 2677 (1972)
18. W. Kleemann, F.J. Schafer, J. Nouet, Linear magnetic birefringence and double-excitonic transitions of the two-dimensional antiferromagnet $BaNiF_4$, Journal of Physics C: Solid State Physics **14**(30), 4447 (1981)
19. J.M. Dance, Nature de l'effet jahn-teller cooperatif dans les fluorures alcalinoterreux $ACuF_4$. Influence sur les proprietes magnetiques, Materials Research Bulletin **16**(5), 599 (1981)
20. A.C. Garcia-Castro, W. Ibarra-Hernandez, E. Bousquet, A.H. Romero, Direct Magnetization-Polarization Coupling in $BaCuF_4$, Physical Review Letters **121**(11) (2018)
21. D.E. Cox, M. Eibschütz, H.J. Guggenheim, L. Holmes, Neutron Diffraction Study of the Magnetic Structure of $BaNiF_4$, Journal of Applied Physics **41**(3), 943 (1970)

22. S. Zhou, J. Wang, Q. Xu, J. Du, The wasp-waisted hysteresis loop and exchange bias in multiferroic $BaNiF_4$, AIP Advances **7**(5), 055827 (2017)
23. C. Ederer, N.A. Spaldin, Electric-field-switchable magnets: The case of $BaNiF_4$, Physical Review B **74**(2), 020401 (2006)
24. Q. Xu, C. Dai, J. Wang, C. Li, Q. Li, J. Du, Enhanced ferromagnetism in $BaNiF_4$ film, Journal of Alloys and Compounds **741**, 265 (2018)
25. M. Welsch, S. Kummer-Dörner, B. Peschel, D. Babel, Kristallstrukturuntersuchungen an den Alkali- und BariumÜbergangsmetallfluoriden RbK2Mn2F7, BaNiF4 und einer 5 : 3-Phase im System BaLiF3/NaCoF3, Zeitschrift für anorganische und allgemeine Chemie **625**(8), 1255 (1999)
26. N.W. Winter, R.M. Pitzer, D.K. Temple, Theoretical study of a Cu^+ ion impurity in a naf host, J. Chem. Phys. **86**, 3549 (1987)
27. A. Gellé, M.B. Lepetit, Fast calculation of the electrostatic potential in ionic crystals by direct summation method, The Journal of Chemical Physics **128**(24), 244716 (2008)
28. A. Gellé, J. Varignon, M.B. Lepetit, Accurate evaluation of magnetic coupling between atoms with numerous open shells: An ab initio method, EPL (Europhysics Letters) **88**(3), 37003 (2009)
29. E. Rebolini, M.B. Lepetit, For an ab initio calculation of the magnetic excitations: Relaxse!, The Journal of Chemical Physics **154**(16), 164116 (2021)
30. B.O. Roos, P.R. Taylor, P.E. Sigbahn, A complete active space scf method (casscf) using a density matrix formulated super-ci approach, Chemical Physics **48**(2), 157 (1980)
31. F. Aquilante, J. Autschbach, R.K. Carlson, L.F. Chibotaru, M.G. Delcey, L. De Vico, I. Fdez. Galván, N. Ferré, L.M. Frutos, L. Gagliardi, M. Garavelli, A. Giussani, C.E. Hoyer, G. Li Manni, H. Lischka, D. Ma, P.A. Malmqvist, T. Müller, A. Nenov, M. Olivucci, T.B. Pedersen, D. Peng, F. Plasser, B. Pritchard, M. Reiher, I. Rivalta, I. Schapiro, J. Segarra-Martí, M. Stenrup, D.G. Truhlar, L. Ungur, A. Valentini, S. Vancoillie, V. Veryazov, V.P. Vysotskiy, O. Weingart, F. Zapata, R. Lindh, Molcas 8: New capabilities for multiconfigurational quantum chemical calculations across the periodic table: Molcas 8, Journal of Computational Chemistry **37**(5), 506 (2016)
32. M. Dolg, H. Stoll, H. Preuss, Ab initio energy-adjusted pseudopotentials for elements of groups 13-17, Theor. Chim. Acta **85**, 441 (1993)
33. L.F. Chibotaru, L. Ungur, Ab initio calculation of anisotropic magnetic properties of complexes. i. unique definition of pseudospin hamiltonians and their derivation, The Journal of Chemical Physics **137**(6), 064112 (2012)
34. G. Radtke, A. Saúl, H.a. Dabkowska, G.M. Luke, G.a. Botton, Interplay between Structural, Electronic, and Magnetic Degrees of Freedom in $Sr_3Cr_2O_8$, Physical Review Letters **105**(3), 036401 (2010)
35. A. Saúl, G. Radtke, Magnetic couplings in $CsV2O_5$: a new picture, Physical Review Letters **106**(17), 177203 (2011)
36. A. Saúl, D. Vodenicarevic, G. Radtke, Theoretical study of the magnetic order in α-CoV_2O_6, Physical Review B **87**(2), 024403 (2013)
37. A. Saúl, G. Radtke, Density functional approach for the magnetism of β-$TeVO_4$, Physical Review B **89**(10), 104414 (2014)
38. G. Radtke, A. Saúl, H.A. Dabkowska, M.B. Salamon, M. Jaime, Magnetic nanopantograph in the $SrCu_2(BO_3)_2$ Shastry–Sutherland lattice, Proceedings of the National Academy of Sciences **112**(7), 1971 (2015)
39. A. Saúl, N. Gauthier, R.M. Askari, M. Côté, T. Maris, C. Reber, A. Lannes, D. Luneau, M. Nicklas, J.M. Law, E.L. Green, J. Wosnitza, A.D. Bianchi, A. Feiguin, Unconventional field induced phases in a quantum magnet formed by free radical tetramers, Physical Review B **97**(6), 064414 (2018)
40. D. Vaclavkova, A. Delhomme, C. Faugeras, M. Potemski, A. Bogucki, J. Suffczynski, P. Kossacki, A. Wildes, B. Gremaud, A. Saul, Magnetoelastic interaction in the two-dimensional magnetic material $MnPS_3$ studied by first principles calculations and Raman experiments, 2D Materials (7), 035030 (2020)
41. P. Blaha, K. Schwarz, F. Tran, R. Laskowski, G.K. Madsen, L.D. Marks, WIEN2k: An APW+lo program for calculating the properties of solids, Journal of Chemical Physics **152**(7) (2020)
42. M. Ernzerhof, G.E. Scuseria, Assessment of the Perdew–Burke–Ernzerhof exchange-correlation functional, The Journal of Chemical Physics **110**(11), 5029 (1999)
43. N. Metropolis, A.W. Rosenbluth, M.N. Rosenbluth, A.H. Teller, E. Teller, Equation of State Calculations by Fast Computing Machines, J. Chem. Phys. **21**, 1087 (1953)
44. N.D. Mermin, H. Wagner, Absence of Ferromagnetism or Antiferromagnetism in One- or Two-Dimensional Isotropic Heisenberg Models, Physical Review Letters **17**(22), 1133 (1966)
45. M.E. Lines, Magnetism in Two Dimensions, Journal of Applied Physics **40**(3), 1352 (1969)
46. T. Yildirim, A.B. Harris, E.F. Shender, Three-dimensional ordering in bct antiferromagnets due to quantum disorder, Phys. Rev. B **53**, 6455 (1996)